

conventional backpropagation with SGD algorithms. We show results training these networks via ADMM and their performance on a supervised feature disentanglement benchmark.

In summary, our paper makes the following contributions:

- We propose Stochastic Block-ADMM for training deep networks. This improves over previous ADMM approaches (in training deep networks) which only work in batch setting.
- We propose an online variant of the Stochastic Block-ADMM for further efficiency in computations.
- We prove the convergence of the proposed Stochastic Block-ADMM algorithm.
- We propose DeepFacto, which jointly trains a non-negative matrix factorization layer with a deep network using ADMM, and show its capability in supervised feature disentanglement.

2 Related Work

Alternating Direction Method of Multipliers (ADMM) has shown promise in solving optimization problems, especially in large-scale and data-distributed machine learning applications. The power of ADMM comes from its decomposition of the augmented Lagrangian into simpler loosely-coupled sub-problems which enables it to solve each sub-problem in an efficient and potentially parallel manner. ADMM extensions for non-convex problems have been recently proposed which are more suitable for large data sets and more complicated problems [Wang *et al.*, 2019b; Huang and Chen, 2018].

A recent line of research has focused on training DNNs using optimization techniques that decompose the training into smaller subproblems, including Block Coordinate Descent (BCD) and ADMM. On the BCD algorithms, [Carreira-Perpinan and Wang, 2014] was the earliest to propose training a DNN in a distributed setting by formulating it as a constrained optimization problem. Further, [Zeng *et al.*, 2019a; Zhang and Brand, 2017; Askari *et al.*, 2018; Gu *et al.*, 2018] lifted the non-convex activations (e.g. ReLU) and formulated the DNN training as a multi-convex problem and solved it using BCD and [Choromanska *et al.*, 2018] proposed an online method for training DNNs.

On the other hand, [Taylor *et al.*, 2016] proposed a batch gradient-free algorithm for training neural networks using a variant of ADMM. However, due to the closed-form update of all the parameters, the proposed method has limitations (e.g. only capable of using simple losses such as Hinge loss and MSE), and cannot be further extended into more complex problems and larger datasets. However, the scope of [Zhang *et al.*, 2016] is limited to a specific application and no convergence proof is presented.

[Gotmare *et al.*, 2018] splits DNNs into blocks and trained them separately by introducing gluing variables. This is very close to ADMM, but it did not use the dual variables common in ADMM and did not present a convergence proof for their method. Recently, [Wang *et al.*, 2019a; Zeng *et al.*, 2019b] have provided convergence analysis of ADMM (to a stationary point) in deep learning by linearly

approximating the non-linear constraints in the DNN training problem. However, their work did not address stochastic gradients as in our work.

Non-negative Matrix Factorization (NMF) imposes non-negativity constraints over the factors, hence can lead to more interpretable decompositions than methods such as Principle Component Analysis (PCA) [Lee and Seung, 1999; Liu *et al.*, 2011]. [Collins *et al.*, 2018] applied NMF over convolutional activations which has shown interpretable and coherent behavior over image parts. However, in their work, NMF was applied post-hoc over pre-trained CNN activations. There is no guarantee that the disentanglement is faithful to the underlying mechanism of the DNN. To the best of our knowledge, NMF layers jointly trained with a deep neural network have not been studied in the past.

3 Method

There were many hurdles in using ADMMs for deep learning — the global convergence proof of the ADMM [Deng and Yin, 2016] assumes that the optimization objective is deterministic and the global solution is calculated at each iteration of the cyclic parameter updates. This typically requires matrix inversion and makes standard ADMM computationally expensive thus impractical for training of many large-scale optimization problems. To see a formulation of standard ADMM for training DNNs refer to the supplementary materials A.

In this section, we present stochastic Block-ADMM which does not require global solution as well as an online version which further reduces the communication load. We prove the convergence of these algorithms in Sec. 3.3 and present its application in supervised disentanglement in Sec. 3.4.

3.1 Stochastic Block-ADMM

In this section, we introduce a novel variant of ADMM for training DNNs, the stochastic block-ADMM. We first split the conventional multi-layer network architectures into an arbitrary number of *blocks*, each containing only a part of the network. To make the parameters of each block independent from its neighbors, *decoupling variables* $\{\mathbf{Z}_t, t = 1, \dots, T\}$ are introduced as shown in Fig. 1(a). These variables pass the information forward and backward in the architecture to train blocks in a cyclic manner until consensus is reached. Each $block_t$ consists of one or multiple differentiable layers (e.g., convolutional layers, activation layers, etc.) that are detached from the rest of the network via coupling variables. Denote the set of all learnable parameters of each $block_t$ as Θ_t . As an example, a $block_t$ wrapping multiple layers can be seen in Figure 1(b). Our formulation is:

$$\underset{\Theta, \mathbf{Z}}{\text{minimize}} \mathcal{J}(\mathbf{Y}, \mathbf{Z}_T) \quad (1)$$

$$\text{subject to } \mathbf{Z}_t = \text{block}_{\Theta_t}(\mathbf{Z}_{t-1}), \quad \mathbf{Z}_0 = \mathbf{X}$$

where $\Theta = \{\Theta_t\}_{t=1}^T$ and $\mathbf{Z} = \{\mathbf{Z}_t\}_{t=1}^T$. \mathcal{J} is the desired cost to be minimized (e.g., cross-entropy loss), T is the total number of blocks, $\mathbf{X} = \{\mathbf{x}_1, \dots, \mathbf{x}_N\} \in \mathbb{R}^{M \times N}$ is the input data, and $\mathbf{Y} = \{\mathbf{y}_1, \dots, \mathbf{y}_N\} \in \mathbb{R}^{C \times N}$ is the target label – for C classes. Note that the number of blocks T can be different than the number of layers in the network L .

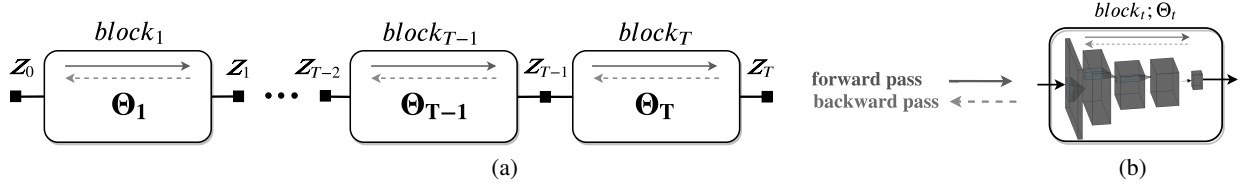


Figure 1: a) General Architecture for training DNNs proposed in Stochastic block-ADMM. b) A few differential layers selected from a parent network are stacked inside a block. The parameters Θ_t are updated by SGD in a forward-backward pass.

To train DNNs with this new approach, we would have the following augmented Lagrangian minimization problem to enforce the equality constraints needed for training,

$$\begin{aligned} \min_{\Theta, \mathbf{Z}} \mathcal{J}(\mathbf{Y}, \mathbf{Z}_T) + \sum_{t=1}^T \frac{\beta_t}{2} \|\mathbf{Z}_t - \text{block}_{\Theta_t}(\mathbf{Z}_{t-1}) + \mathbf{U}_t\|_F^2 \\ \text{subject to } \mathbf{Z}_0 = \mathbf{X} \end{aligned} \quad (2)$$

where β_t and \mathbf{U}_t are the (scaled) step size and the Lagrange multiplier corresponding to the t -th Block, respectively. Our proposed Stochastic block-ADMM method for training problem (2) is presented in Algorithm 1. ζ_t and η_t are the learning rates in each update step for \mathbf{Z}_t and Θ_t , respectively. Similar to training conventional neural networks, each block is updated by first going in a forward pass through the block and update the parameters using back-propagation. Update of the block parameters Θ_t is done using mini-batch stochastic gradient descent or Adam. The same goes for the decoupling variables \mathbf{Z}_t . Note, in each cycle of the parameter update in Algorithm 1, all the samples of \mathbf{Z} are updated, while Θ_t is updated stochastically. In addition, due to non-convexity of primal sub-problem (Eq. 5a), one can perform the primal updates for multiple steps. In Algorithm 1, we take the reverse order for updating the decoupling variables \mathbf{Z}_t , which we have empirically found more efficient, as analogous to backpropagation where gradient flows backwards as well.

Note that in this formulation, backpropagation stops at each auxiliary variable \mathbf{Z}_t . Hence, our method can readily mitigate the long-known vanishing gradient problem by splitting a conventional DNN into arbitrary sized blocks. During testing time, one could follow Eq. (2) to solve an optimization problem. But in practice, it suffices to use a straight-through estimator by removing the decoupling variables and simply pass the output of each layer to the next, equivalent of doing a forward pass in a conventional DNN.

3.2 Online Stochastic Block-ADMM

The stochastic block-ADMM formulation in section 3.1 is still a batch mode algorithm, in the sense that the entire training set is updated at once. This imposes restrictions on the size of the input and the number of parameters in the network when limited resources are available. Also, it does not readily accommodate to settings where data is constantly changing, such as data augmentation on the input or reinforcement learning. To overcome such limitations, we propose an *online* variant of the stochastic block-ADMM in Algorithm 2 which

Algorithm 1 Stochastic Block-ADMM

Input: data \mathbf{X} , labels \mathbf{Y}
Params: $\beta_t > 0, \zeta_t > 0, \eta_t > 0$
Define: $\mathcal{T}(\mathbf{Z}_t, \mathbf{Z}_{t-1}, \mathbf{U}_t, \Theta_t) = \frac{\beta_t}{2} \|\mathbf{Z}_t - \text{block}_{\Theta_t}(\mathbf{Z}_{t-1}) + \mathbf{U}_t\|_F^2$
Initialize: $\{\Theta_t^0\}_{t=1}^T, \{\mathbf{U}_t^0\}_{t=1}^T, k \leftarrow 0$
Initialize: $\{\mathbf{Z}_t\}_{t=1}^T$ in a forward pass.
repeat
 $\mathbf{Z}_T^{k+1} \leftarrow \mathbf{Z}_T^k - \zeta_T \nabla_{\mathbf{Z}_T^k} (\mathcal{J}(\mathbf{Y}_i, \mathbf{Z}_T^k) + \mathcal{T}(\mathbf{Z}_T^k, \mathbf{Z}_{T-1}^k, \mathbf{U}_T^k, \Theta_T^k))$
for $t = T - 1$ **to** 1 **do**
 $\mathbf{Z}_t^{k+1} \leftarrow \mathbf{Z}_t^k - \zeta_t \nabla_{\mathbf{Z}_t^k} (\mathcal{T}(\mathbf{Z}_t^k, \mathbf{Z}_{t-1}^k, \mathbf{U}_t^k, \Theta_t^k) + \mathcal{T}(\mathbf{Z}_{t+1}^{k+1}, \mathbf{Z}_t^k, \mathbf{U}_{t+1}^k, \Theta_{t+1}^k))$
end for
for $t = 1$ **to** T **do**
 $\Theta_t^{k+1} \leftarrow \Theta_t^k - \eta_t \nabla_{\Theta_t} \mathcal{T}(\mathbf{Z}_{t,i}^{k+1}, \mathbf{Z}_{t-1,i}^{k+1}, \mathbf{U}_{t,i}^k, \Theta_t^k)$,
draw $i \subset \{1, \dots, N\}$
 $\mathbf{U}_t^{k+1} \leftarrow \mathbf{U}_t^k + \mathbf{Z}_t^{k+1} - \text{block}_{\Theta_t^{k+1}}(\mathbf{Z}_{t-1}^{k+1})$
end for
until some stopping criterion is reached.

alternatively solves the unconstrained problem,

$$\begin{aligned} \min_{\Theta, \mathbf{Z}} \mathcal{J}(\mathbf{y}, \mathbf{z}_T) + \sum_{t=1}^T \frac{\beta_t}{2} (\|\mathbf{z}_t - \text{block}_{\Theta_t}(\mathbf{z}_{t-1})\|_F^2 + u_t) \\ \text{subject to } \mathbf{z}_0 = \mathbf{x} \end{aligned} \quad (3)$$

Although similar to the Eq. (2), the dual variable in the online Block-ADMM is a *scalar*. The benefits of this are two-folded: First, this substantially reduces the memory size needed for storing the dual variables as the optimization proceeds. Second, this considerably reduces the variance in the gradient induced by re-initializing the auxiliary variables $\mathbf{z}_{\ell,i}$ when updating the block parameters at each iteration.

3.3 Convergence of the Algorithm

Let us consider the following general problem:

$$\begin{aligned} \underset{\mathcal{Z}, \Theta}{\text{minimize}} f(\mathcal{Z}) \\ \text{subject to } h(\mathcal{Z}, \Theta) = \mathbf{0}, \end{aligned} \quad (4)$$

where \mathcal{Z} and Θ are as defined in Sec. 3.1, and $f(\cdot)$ represents the training objective, and $h(\cdot)$ represents the layer coupling equalities as in eq. (1). We also assume that both $f(\cdot)$ and $h(\cdot)$ are differentiable functions. Note that both f and h can be non-convex.

Algorithm 2 Online Stochastic Block-ADMM

Input: data \mathbf{X} , labels \mathbf{Y}
Params: $\beta_t > 0$, $\zeta_t > 0$, $\eta_t > 0$
Define: $\mathcal{T}(\mathbf{z}_t, \mathbf{z}_{t-1}, u_t, \Theta_t) = \frac{\beta_t}{2} (\|\mathbf{z}_t - \text{block}_{\Theta_t}(\mathbf{z}_{t-1})\|_2 + u_t)^2$
Initialize: $\{\Theta_t^0\}_{t=1}^T$, $\{u_t^0\}_{t=1}^T$, $k \leftarrow 0$
repeat
 for $(\mathbf{x}_i, \mathbf{y}_i)$ **in** (\mathbf{X}, \mathbf{Y}) **do**
 Initialize: $\{\mathbf{z}_{t,i}\}_{i=1}^T$ in a forward pass ($\mathbf{z}_{0,i} = \mathbf{x}_i$).
 $\mathbf{z}_{T,i} \leftarrow \mathbf{z}_{T,i} - \zeta_T \nabla_{\mathbf{z}_{T,i}} (\mathcal{J}(\mathbf{y}_i, \mathbf{z}_{T,i})$
 $+ \mathcal{T}(\mathbf{z}_T, \mathbf{z}_{T-1}, u_T^k, \Theta_T^k))$
 for $t = T - 1$ **to** 1 **do**
 $\mathbf{z}_{t,i} \leftarrow \mathbf{z}_{t,i} - \zeta_t \nabla_{\mathbf{z}_{t,i}} (\mathcal{T}(\mathbf{z}_{t,i}, \mathbf{z}_{t-1,i}, u_t^k, \Theta_t^k)$
 $+ \mathcal{T}(\mathbf{z}_{t+1,i}, \mathbf{z}_{t,i}, u_{t+1}^k, \Theta_{t+1}^k))$
 end for
 for $t = 1$ **to** T **do**
 $\Theta_t^{k+1} \leftarrow \Theta_t^k - \eta_t \nabla_{\Theta_t} \mathcal{T}(\mathbf{z}_{t,i}, \mathbf{z}_{t-1,i}, u_t^k, \Theta_t^k)$
 $u_t^{k+1} \leftarrow u_t^k + \|\mathbf{z}_t^k - \text{block}_{\Theta_t^{k+1}}(\mathbf{z}_{t-1,i})\|_2$
 end for
 end for
until some stopping criterion is reached.

Let us consider the following augmented Lagrangian:

$$\mathcal{L}_{\rho_k}(\mathcal{Z}, \Theta, \lambda) = f(\mathcal{Z}) + \langle \lambda, h(\mathcal{Z}, \Theta) \rangle + \frac{1}{2\rho_k} \|h(\mathcal{Z}, \Theta)\|_2^2,$$

where λ collects all the dual variables $\mathbf{U}_1, \dots, \mathbf{U}_T$ that correspond to different layers. The standard primal-dual updates can be summarized as follows:

$$(\mathcal{Z}^{k+1}, \Theta^{k+1}) \leftarrow \arg \min_{\mathcal{Z}, \Theta} \mathcal{L}_{\rho_k}(\mathcal{Z}, \Theta, \lambda^k), \quad (5a)$$

$$\lambda^{k+1} \leftarrow \lambda^k + \frac{1}{\rho_k} h(\mathcal{Z}^{k+1}, \Theta^{k+1}), \quad (5b)$$

We employ the trick in [Shi *et al.*, 2017] for adaptively adjusting the parameter ρ_k . We assume that ρ_k is adjusted by

$$\rho_{k+1} \leftarrow \begin{cases} \rho_k, & \|h(\mathcal{Z}^k, \Theta^k)\| \leq \eta_k, \\ c\rho_k, & 0 < c < 1, \quad \text{o.w.} \end{cases} \quad (6)$$

where η_k for $k = 1, 2, \dots$ is a pre-specified sequence that bounds the equality-enforcing error.

Our analysis shows the following convergence result:

Proposition 1 *Assume $h(\mathcal{Z}, \Theta) = \mathbf{0}$ satisfies the Robinson’s condition. Also assume for each update in eq. (5a), the sub-problem solution solved by stochastic alternating optimization satisfies*

$$\mathbb{E} \left[\|\mathcal{G}(\mathbf{x}^k)\|^2 \right] \leq \varepsilon_k, \quad \mathbb{V} [\mathcal{G}(\mathbf{x}^k)] \leq \sigma_k^2, \quad (7)$$

where $\mathbf{x} = (\mathcal{Z}, \Theta)$ is a vector that collects all the optimization variables and $\mathcal{G}(\mathbf{x}^k)$ collects the stochastic gradients that we used for updating (\mathcal{Z}, Θ) . Assume that the stochastic gradient for the primal update is unbiased, i.e.,

$$\mathbb{E}[\mathcal{G}(\mathbf{x}^k)] = \nabla \mathcal{L}_{\rho_k}(\mathbf{x}_k), \quad \forall k. \quad (8)$$

Then, every limit point of the solution sequence produced by the algorithm in eq. (5) converges to a KKT point of the problem in eq. (4), if $\eta_k \rightarrow 0$, $\sigma_k^2 \rightarrow 0$ and $\varepsilon_k \rightarrow 0$.

The proof for Proposition 1 is presented in the supplementary materials B. Proposition 1 asserts that the algorithm converges to a KKT point under some conditions. There are a number of remarks regarding implementation. To begin with, the condition $\varepsilon_k \rightarrow 0$ means that the primal problem needs to be solved more and more accurately when k grows, in terms of approaching the stationary point of the sub-problem using block stochastic gradient. This can be achieved via gradually increasing the number of iterations for the primal updates. Note that stochastic block gradient can provably attain $\mathbb{E}[\|\mathcal{G}(\mathbf{X}^k)\|^2] \leq \varepsilon_k$; see [Xu and Yin, 2015].

3.4 DeepFacto: Factorization of DNN Activations

Here, we investigate a task for supervised disentanglement, which can provide insights for explaining DNNs to humans. Supervised disentanglement aims to find disentangled factors that decide the CNN output, yet are human-understandable and distinct from each other. One approach to learn a disentangled representation is through adding non-negative matrix factorization (NMF)[Lee and Seung, 1999] layers to the network [Collins *et al.*, 2018]. Note that NMF imposes non-differentiable constraints into the network where conventional end-to-end training using backpropagation would not be applicable. Hence, prior work were mostly running NMF after the training, where the network might have already learned highly entangled features. In this work, aided with our stochastic block-ADMM, we attempt to perform training with NMF layers in the intermediate layers of DNNs.

Figure 2 shows an *NMF module* with rank r incorporated between two arbitrary neighboring blocks. The output from the *block_t* is factorized into \mathbf{M}_t and \mathbf{S}_t , namely, the basis and score matrices. In this configuration, only the score matrix \mathbf{S}_t is passed to the next blocks. The score matrix is low-rank, sparse and non-negative hence can possibly represent features that are more disentangled than the original network. Exploring this architecture is one attempt of us in making deep networks more explainable to humans. Humans would not be able to interpret conventional deep network weights which are both positive and negative and sometimes cancels out each other. The sparse and non-negative feature from NMF would be much more preferable to interpret [Collins *et al.*, 2018].

However, the NMF module breaks the gradient path from \mathbf{S}_t to \mathbf{Z}_t , hence conventional backpropagation would not be applicable in this problem. We extend the ADMM framework (2) into having non-negative factorization constraints over its activations and formulate the following optimization problem:

$$\begin{aligned} & \min_{\Theta, \mathcal{Z}, \mathbf{S}, \mathbf{M}} \mathcal{J}(\mathbf{Y}, \mathbf{Z}_T) \\ & + \sum_{k=1, k \neq t+1}^T \frac{\beta_k}{2} \|\mathbf{Z}_k - \text{block}_k(\mathbf{Z}_{k-1}) + \mathbf{U}_k\|_F^2 \\ & + \frac{\beta_{t+1}}{2} \|\mathbf{Z}_{t+1} - \text{block}_{t+1}(\mathbf{S}_t) + \mathbf{U}_{t+1}\|_F^2 \\ & + \frac{\gamma_t}{2} \|\mathbf{Z}_t - \mathbf{M}_t \mathbf{S}_t + \mathbf{V}_t\|_F^2 \\ & \quad \forall i, j \mathbf{M}_{\ell, ij} \geq 0, \mathbf{S}_{\ell, ij} \geq 0 \end{aligned} \quad (9)$$

where γ_t is the step-size and \mathbf{V}_t is the corresponding multipliers to enforce the matrix factorization equality $\mathbf{Z}_t = \mathbf{M}_t \mathbf{S}_t$. The NMF module adds a nonconvex term to the optimization. However, in the alternating optimization scheme, while

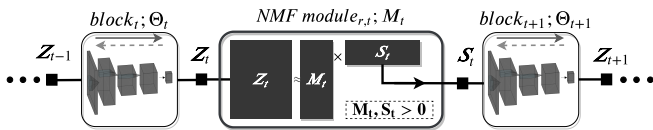


Figure 2: General architecture for Deepfacto: an NMF module with rank r is added in the middle of two arbitrary blocks. Note, only S_t is passed to the next blocks.

keeping either M_t or S_t constant, solving for the other term would reduce to a normal convex least-squares problem. The rest of the updates are the same as in section 3.1. Note that, trivially to not change the input dimension of the next block after the NMF module, one can simply add an affine layer to increase the dimensions without changing the formulation.

At testing time, one only needs to perform a non-negative projection since the basis matrix M will be given, which can be solved using a convex solver such as LBFSGS. Note that for simplicity, we only formulated adding *one* NMF module in the middle of the blocks. This can be simply extended to as many NMF modules as needed in the architecture.

4 Experiments

All the experiments are run on a machine with a single NVIDIA GeForce RTX 2080 Ti GPU. The results presented for each of the following experiments are selected from their best performance after grid search over the hyper-parameters, both for our method and the baselines. Each algorithm is ran five times with different initialization and the average test set accuracy is reported. The shaded area corresponds to ± 1 standard deviation. We will make our code available online.

4.1 Supervised Deep Network Training

In this section, we present the experiment results from training conventional neural networks in a supervised setting on the MNIST, Fashion-MNIST, and CIFAR-10 datasets. For experiments results on Fashion-MNIST and CIFAR-10, see supplementary materials C.

MNIST

For the first supervised learning experiment, the MNIST dataset of handwritten digits [Yann LeCun,], is used for the evaluation of ADMM/BCD methods for training DNNs. We use the standard train/test split. The performance on the testing set of 10,000 samples is reported in Figure 3. The architecture of the *shallow* network used for the experiments incorporates three fully-connected layers with 128-neuron hidden layers (784–128–128–10) and *ReLU* nonlinearity. In order to make a fair comparison with [Taylor *et al.*, 2016] which can only work with Mean Squared Error (MSE), we utilize MSE as the training objective (\mathcal{J}) while the more common Cross-Entropy (CE) is applicable in our block-ADMM formulation and utilized in the experiments in the supplementary materials.

In training standard ADMM and [Taylor *et al.*, 2016] as baselines, all the parameters are initialized by sampling from the uniform distribution $x \sim U(0, 10^{-4})$. We set $\beta_l = \gamma_l =$

10 for all of the layers. Weight decay is used with $\lambda_l = 5 \times 10^{-5}$. For baselines with backpropagation in Fig. 3, a learning rate of 5×10^{-3} is used.

Further, for the training of the batch and online Stochastic Block-ADMM algorithms presented in Algorithm 1 and 2, the aforementioned three-layer architecture is split into 3 one-layer blocks. β_t is set to 1 for all layers, the weights are initialized using the normal distribution, dual variables U_t are initialized using a uniform distribution, and auxiliary variables Z_t are initialized in a forward pass. During training, the block parameters (Θ_t) are updated stochastically, and both of sub-problem updates for the block $_{\Theta_t}$ and Z_t are performed using *Adam*. In our experiments in the batch mode, we performed the primal updates for 3 steps during each iteration. For the online version, we set the batch size to 64 and auxiliary variables are re-initialized at each iteration (see Algorithm 2).

Figure 3 shows that Stochastic Block-ADMM outperforms the baselines by reaching 97.61% average test accuracy. Note the accuracy for all methods is lower than normal because of the MSE loss function that is used — which is not the best choice for classification yet chosen for fair comparison with previous ADMM methods. The online version performs slightly worse with a 93.88% test accuracy. However, this comes with enormous advantage in terms of memory utilization, e.g. given the configuration for training on MNIST, the online version uses $10\times$ less memory to store training variables compared to the batch version.

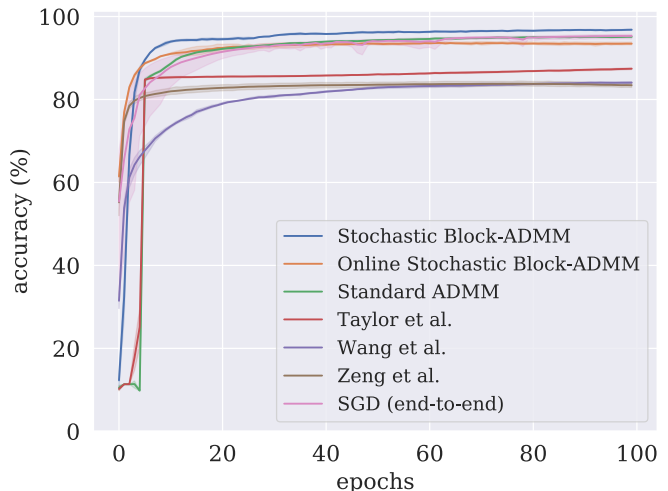


Figure 3: Test set accuracy on MNIST using network with 3 fully-connected layers: 784 – 128 – 128 – 10. Final test accuracy: “Stochastic Block-ADMM”: **97.61%**, “Online Stochastic Block-ADMM”: 93.88%, “Standard ADMM”: 95.02%, [Taylor *et al.*, 2016]: 87.52%, [Wang *et al.*, 2019a]: 83.89%, [Zeng *et al.*, 2019a]: 83.28% , “SGD”: 95.29% (Best viewed in color)

Vanishing Gradient

Since no gradient is backpropagated through the entire network in our proposed algorithm, stochastic block-ADMM is robust against vanishing gradients. We run the previous ex-

periments on an unconventional architecture with 10 fully-connected layers — this is to make the vanishing gradient problem obvious. Note that normally this will not be adopted because of the severe overfitting and gradient vanishing problems, but here we utilized this setting to test our resistance to these problems. Figure 4 illustrates the experiment results. Stochastic Block-ADMM reaches final test accuracy of 94.43% while SGD and ADAM only reach to 10.28% and 58%, respectively. As it can be seen in Figure 4, we also compared our method with the recent work of [Zeng *et al.*, 2019a]. We observed the BCD in [Zeng *et al.*, 2019a] to be unstable, sensitive to network architectures, and eventually, not converging after 300 epochs. Although we still exhibited some overfitting, we can see our approach is significantly better in handling of the vanishing gradient problem, and performs reasonably well. We further tested our performance with 20 fully-connected layers. Results show that although there is slightly more overfitting, our algorithm can still find a reasonable solution (Fig. 4), showing its potential in helping with training scenarios with vanishing gradients.

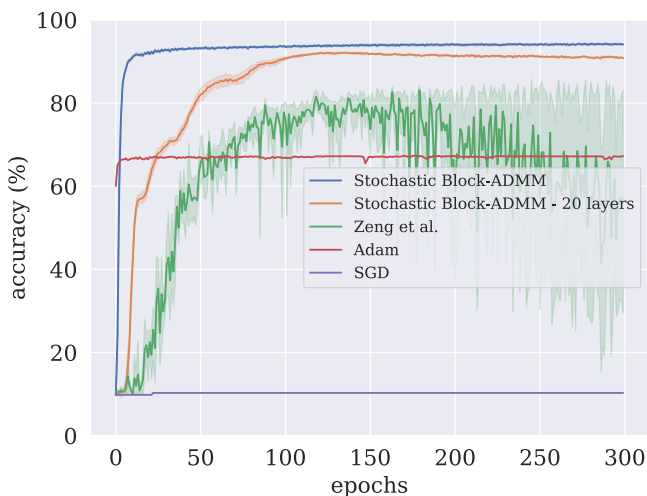


Figure 4: Test accuracies from deep architectures on MNIST. Block-ADMM demonstrates stable convergence and obtains final test accuracy of **94.43%** (10 layers), and 91.75% (20 layers) respectively, while SGD and Adam (10 layers) fail due to vanishing gradients (Best viewed in color)

Wall Clock Time Comparison

In this section, we analyze the batch and online versions of stochastic block-ADMM in training wall clock time and compare them against other baselines as illustrated in Figure 5. Note Gotmare *et al.* and SGD are trained with a mini-batch size of 64 and [Zeng *et al.*, 2019a; Wang *et al.*, 2019a] are trained in a batch setting. Only the time taken for the *training* was plotted in Fig. 5 and stages such as initialization, data loading, etc were excluded. The online version shows faster convergence than [Gotmare *et al.*, 2018] and simple SGD. Although [Zeng *et al.*, 2019a] and [Wang *et al.*, 2019b] have been convergence rates due to being batch methods, our approach achieves higher performance later on.

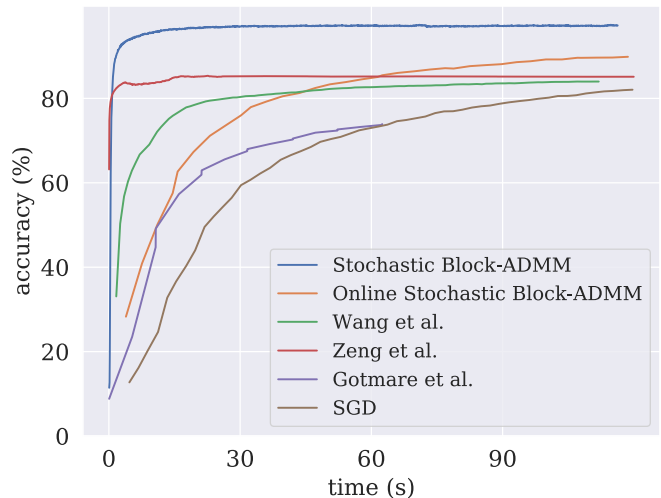


Figure 5: Test set accuracy v.s. training wall clock time comparison of different alternating optimization methods for training DNNs on the MNIST dataset. Our methods (blue and orange) show superior performance vs. [Zeng *et al.*, 2019a] and [Wang *et al.*, 2019b] while converge faster than all other methods

4.2 Supervised Disentangling on LFWA

In this section, we showcase the flexibility of stochastic block-ADMM in training deep networks with non-differentiable layers where conventional backpropagation cannot be used. For that purpose, we evaluate our proposed method in a supervised disentanglement problem where we used DeepFacto 3.4 to learn a nonnegative factorized representation of the DNN activations while training end-to-end on the LFWA dataset [Huang *et al.*, 2007]. Next, similar to [Liu *et al.*, 2018], linear SVMs are used over the factorized space to predict face attributes. This setup examines the capability of the network to extract a disentangled representation that linearly corresponds to human-marked attributes that the network does not have prior knowledge of.

We used the Inception-Resnet architecture from [Schroff *et al.*, 2015], pre-trained on the VGGFace-2 [Cao *et al.*, 2018] dataset as the back-bone. To incorporate an NMF, we follow the same approach as in Fig. 2 where the pretrained DNN is the first block, and we add a simple fully-connected layer over the score matrix S_t to train a face-verification network with a triplet loss [Hoffer and Ailon, 2015]. We conjecture the score matrix S_t will be guided to learn an disentangled factorization due to the nonnegativity constraint [Collins *et al.*, 2018]. To have a warm start for an end-to-end training of DeepFacto, we first pre-train the NMF module having the Inception-Resnet block frozen. Then, we fine-tune the block parameters as well as the NMF module in an alternating fashion, similar to Algorithm 1. Note, the rank of the NMF in DeepFacto is a hyperparameter and we selected three different values ($r = 4, 32, 256$) in the experiments. The final $r = 256$ is also the latent space dimensionality in [Liu *et al.*, 2018]. Table. 1 illustrates average prediction accuracy over LFWA attributes from DeepFacto and other supervised and weakly supervised baselines. This validates that DeepFacto

Table 1: Average prediction accuracy on 40 attributes from LFWA dataset. Weakly-supervised methods train the network without access to attribute labels. Final classification then comes from a linear SVM on their latent representations.

LFWA	ACCURACY
[ZHANG <i>et al.</i> , 2014] (SUPERVISED)	81.00%
[LIU <i>et al.</i> , 2015] (SUPERVISED)	84.00%
[LIU <i>et al.</i> , 2018] (WEAKLY-SUPERVISED)	83.16%
DEEPPFACTO - RANK 4 (WEAKLY-SUPERVISED)	74.80%
DEEPPFACTO - RANK 32 (WEAKLY-SUPERVISED)	81.39%
DEEPPFACTO - RANK 256 (WEAKLY-SUPERVISED)	87.03%

has learned a meaningful representation of the attributes by disentangling the activations. To see visualization for individual dimensions learned by DeepFacto see supplementary materials D.

5 Conclusion and Discussion

In this paper, we proposed stochastic block-ADMM as an approach to train deep networks. Through updates with stochastic gradients, we improve over the capabilities to scale to larger networks using ADMM, as well as the performance. We also presented an online version of stochastic block-ADMM for setting where computational power is limited, or when accessing to all data at once is not practical. We have shown improvements over SGD/Adam in training deep networks without residual connections. As an illustration to how ADMM can be applied in supervised feature disentanglement, we propose DeepFacto which jointly trains an NMF layer within a deep network and show encouraging results on a supervised disentanglement benchmark, both quantitatively and qualitatively. We believe the results presented in this work set up future work that further explores aspects of utilizing ADMM in deep network training, including parallelization and stability.

References

- [Askari *et al.*, 2018] Armin Askari, Geoffrey Negiar, Rajiv Sambharya, and Laurent El Ghaoui. Lifted neural networks. *arXiv preprint arXiv:1805.01532*, 2018.
- [Boyd *et al.*, 2011] Stephen Boyd, Neal Parikh, Eric Chu, Borja Peleato, Jonathan Eckstein, et al. Distributed optimization and statistical learning via the alternating direction method of multipliers. *Foundations and Trends® in Machine Learning*, 3(1):1–122, 2011.
- [Cao *et al.*, 2018] Q. Cao, L. Shen, W. Xie, O. M. Parkhi, and A. Zisserman. Vggface2: A dataset for recognising faces across pose and age. In *International Conference on Automatic Face and Gesture Recognition*, 2018.
- [Carreira-Perpinan and Wang, 2014] Miguel Carreira-Perpinan and Weiran Wang. Distributed optimization of deeply nested systems. In *Artificial Intelligence and Statistics*, pages 10–19, 2014.
- [Choromanska *et al.*, 2018] Anna Choromanska, Benjamin Cowen, Sadhana Kumaravel, Ronny Luss, Mattia Rigotti, Irina Rish, Brian Kingsbury, Paolo DiAchille, Viatcheslav Gurev, Ravi Tejwani, et al. Beyond backprop: Online alternating minimization with auxiliary variables. *arXiv preprint arXiv:1806.09077*, 2018.
- [Collins *et al.*, 2018] Edo Collins, Radhakrishna Achanta, and Sabine Sussstrunk. Deep feature factorization for concept discovery. In *Proceedings of the European Conference on Computer Vision (ECCV)*, pages 336–352, 2018.
- [Deng and Yin, 2016] Wei Deng and Wotao Yin. On the global and linear convergence of the generalized alternating direction method of multipliers. *Journal of Scientific Computing*, 66(3):889–916, 2016.
- [Fu *et al.*, 2018] Xiao Fu, Kejun Huang, Nicholas D Sidiropoulos, Qingjiang Shi, and Mingyi Hong. Anchor-free correlated topic modeling. *IEEE transactions on pattern analysis and machine intelligence*, 41(5):1056–1071, 2018.
- [Gabay and Mercier,] Daniel Gabay and Bertrand Mercier. *A dual algorithm for the solution of non linear variational problems via finite element approximation*.
- [Gotmare *et al.*, 2018] Akhilesh Gotmare, Valentin Thomas, Johanni Brea, and Martin Jaggi. Decoupling backpropagation using constrained optimization methods. 2018.
- [Gu *et al.*, 2018] Fangda Gu, Armin Askari, and Laurent El Ghaoui. Fenchel lifted networks: A lagrange relaxation of neural network training. *arXiv preprint arXiv:1811.08039*, 2018.
- [He *et al.*, 2016] Kaiming He, Xiangyu Zhang, Shaoqing Ren, and Jian Sun. Deep residual learning for image recognition. In *Proceedings of the IEEE conference on computer vision and pattern recognition*, pages 770–778, 2016.
- [Hoffer and Ailon, 2015] Elad Hoffer and Nir Ailon. Deep metric learning using triplet network. In *International Workshop on Similarity-Based Pattern Recognition*, pages 84–92. Springer, 2015.
- [Huang and Chen, 2018] Feihu Huang and Songcan Chen. Mini-batch stochastic admm for nonconvex nonsmooth optimization. 2018.
- [Huang *et al.*, 2007] Gary B. Huang, Manu Ramesh, Tamara Berg, and Erik Learned-Miller. Labeled faces in the wild: A database for studying face recognition in unconstrained environments. Technical Report 07-49, University of Massachusetts, Amherst, October 2007.
- [Kingma and Ba, 2014] Diederik P Kingma and Jimmy Ba. Adam: A method for stochastic optimization. *arXiv preprint arXiv:1412.6980*, 2014.
- [Krizhevsky *et al.*,] Alex Krizhevsky, Vinod Nair, and Geoffrey Hinton. Cifar-10 (canadian institute for advanced research).
- [Lee and Seung, 1999] Daniel D Lee and H Sebastian Seung. Learning the parts of objects by non-negative matrix factorization. *Nature*, 401(6755):788, 1999.
- [Liu *et al.*, 2011] Haifeng Liu, Zhaohui Wu, Xuelong Li, Deng Cai, and Thomas S Huang. Constrained nonnegative matrix factorization for image representation. *IEEE Transactions on Pattern Analysis and Machine Intelligence*, 34(7):1299–1311, 2011.
- [Liu *et al.*, 2015] Ziwei Liu, Ping Luo, Xiaogang Wang, and Xiaoou Tang. Deep learning face attributes in the wild. In *Proceedings of the IEEE international conference on computer vision*, pages 3730–3738, 2015.
- [Liu *et al.*, 2018] Yu Liu, Fangyin Wei, Jing Shao, Lu Sheng, Junjie Yan, and Xiaogang Wang. Exploring disentangled feature representation beyond face identification. In *Proceedings of the IEEE*

- Conference on Computer Vision and Pattern Recognition*, pages 2080–2089, 2018.
- [Schroff *et al.*, 2015] Florian Schroff, Dmitry Kalenichenko, and James Philbin. Facenet: A unified embedding for face recognition and clustering. In *Proceedings of the IEEE conference on computer vision and pattern recognition*, pages 815–823, 2015.
- [Shi *et al.*, 2017] Qingjiang Shi, Mingyi Hong, Xiao Fu, and Tsung-Hui Chang. Penalty dual decomposition method for nonsmooth nonconvex optimization. *arXiv preprint arXiv:1712.04767*, 2017.
- [Taylor *et al.*, 2016] Gavin Taylor, Ryan Burmeister, Zheng Xu, Bharat Singh, Ankit Patel, and Tom Goldstein. Training neural networks without gradients: A scalable admm approach. In *International conference on machine learning*, pages 2722–2731, 2016.
- [Wang *et al.*, 2019a] Junxiang Wang, Fuxun Yu, Xiang Chen, and Liang Zhao. Admm for efficient deep learning with global convergence. In *Proceedings of the 25th ACM SIGKDD International Conference on Knowledge Discovery & Data Mining*, pages 111–119, 2019.
- [Wang *et al.*, 2019b] Yu Wang, Wotao Yin, and Jinshan Zeng. Global convergence of admm in nonconvex nonsmooth optimization. *Journal of Scientific Computing*, 78(1):29–63, 2019.
- [Xu and Yin, 2015] Yangyang Xu and Wotao Yin. Block stochastic gradient iteration for convex and nonconvex optimization. *SIAM Journal on Optimization*, 25(3):1686–1716, 2015.
- [Yann LeCun,] Christopher J.C. Burges Yann LeCun, Corinna Cortes. THE MNIST DATABASE of handwritten digits.
- [Zeng *et al.*, 2019a] Jinshan Zeng, Tim Tsz-Kit Lau, Shaobo Lin, and Yuan Yao. Global convergence of block coordinate descent in deep learning. In *International Conference on Machine Learning*, pages 7313–7323, 2019.
- [Zeng *et al.*, 2019b] Jinshan Zeng, Shao-Bo Lin, and Yuan Yao. A convergence analysis of nonlinearly constrained admm in deep learning. *arXiv preprint arXiv:1902.02060*, 2019.
- [Zhang and Brand, 2017] Ziming Zhang and Matthew Brand. Convergent block coordinate descent for training tikhonov regularized deep neural networks. In *Advances in Neural Information Processing Systems*, pages 1721–1730, 2017.
- [Zhang *et al.*, 2014] Ning Zhang, Manohar Paluri, Marc’Aurelio Ranzato, Trevor Darrell, and Lubomir Bourdev. Panda: Pose aligned networks for deep attribute modeling. In *Proceedings of the IEEE conference on computer vision and pattern recognition*, pages 1637–1644, 2014.
- [Zhang *et al.*, 2016] Ziming Zhang, Yuting Chen, and Venkatesh Saligrama. Efficient training of very deep neural networks for supervised hashing. In *Proceedings of the IEEE conference on computer vision and pattern recognition*, pages 1487–1495, 2016.

Supplementary Materials

A Background: Standard ADMM Training of DNNs

Alternating Direction Method of Multipliers (ADMM) [Gabay and Mercier, ; Boyd *et al.*, 2011] is a class of optimization methods belonging to *operator splitting techniques* which borrows benefits from both dual decomposition and augmented Lagrangian methods for constrained optimization.

To formulate training an L -layer DNN in a general supervised setting, we would have the following non-convex constrained optimization problem [Zeng *et al.*, 2019a]:

$$\begin{aligned} & \underset{\mathcal{W}, \mathcal{A}, \mathcal{Z}}{\text{minimize}} && \mathcal{J}(\mathbf{Y}, \mathbf{Z}_L) + \sum_{\ell=1}^L \lambda_{\ell} \mathbf{r}_{\ell}(\mathbf{W}_{\ell}) && (10) \\ & \text{subject to} && \mathbf{A}_{\ell} - \phi_{\ell}(\mathbf{Z}_{\ell}) = \mathbf{0}, \quad \ell = 1, \dots, L-1 \\ & \text{subject to} && \mathbf{Z}_{\ell} - \mathbf{W}_{\ell} \mathbf{A}_{\ell-1} = \mathbf{0}, \quad \ell = 1, \dots, L \end{aligned}$$

where \mathcal{J} is the main objective (*e.g.*, cross-entropy, mean-squared-error loss functions) that needs to be minimized. The subscript ℓ denotes the ℓ -th layer in the network. The optimization variables are $\mathcal{W} = \{\mathbf{W}_{\ell}\}_{\ell=1}^L$, $\mathcal{A} = \{\mathbf{A}_{\ell}\}_{\ell=1}^{L-1}$, and $\mathcal{Z} = \{\mathbf{Z}_{\ell}\}_{\ell=1}^L$ where \mathbf{W}_{ℓ} , \mathbf{Z}_{ℓ} , \mathbf{A}_{ℓ} , and $\phi_{\ell}(\cdot)$ are the weight matrix, output matrix, activation matrix, and the activation function (*e.g.*, ReLU) at the ℓ -th layer, respectively. Note that $\mathbf{A}_0 = \mathbf{X}$ where $\mathbf{X} = \{\mathbf{x}_1, \dots, \mathbf{x}_N\} \in \mathbb{R}^{M \times N}$ is the input data matrix containing N samples with input dimensionality M ; $\mathbf{Y} = \{\mathbf{y}_1, \dots, \mathbf{y}_N\} \in \mathbb{R}^{C \times N}$ is the target matrix pair comprised of N one-hot vector label of dimension C , representing number of prediction classes. Also, $\mathbf{r}(\cdot)$ is the regularization term with (*e.g.*, Frobenius norm $\|\cdot\|_F^2$) corresponding penalty weight λ_{ℓ} . Note that the regularization term can be simply ignored by setting λ_{ℓ} to zero. In this formulation, the intercept in each layer is ignored for simplicity as it can be simply be added by slightly modifying the \mathbf{W}_{ℓ} and the input to each layer. The formulation in Eq. (10) breaks the the conventional multi-layer backpropagation optimization of DNNs into simpler sub-problems that can be solved efficiently (*e.g.* reducing to least-squares problem). This also facilitates training in a distributed manner — as the layers of the DNN are decoupled and the variables can be updated in parallel across layers (\mathbf{W}_{ℓ}) and data points ($\mathbf{W}_{\ell}, \mathbf{Z}_{\ell}, \mathbf{A}_{\ell}$).

To enforce the constraints in problem (10) and solve the optimization using ADMM, we would have the following augmented Lagrangian problem:

$$\begin{aligned} & \underset{\mathcal{W}, \mathcal{A}, \mathcal{Z}}{\text{minimize}} && \mathcal{J}(\mathbf{Y}, \mathbf{Z}_L) + \sum_{\ell=1}^L \lambda_{\ell} \mathbf{r}_{\ell}(\mathbf{W}_{\ell}) && (11) \\ & && + \sum_{\ell=1}^L \frac{\beta_{\ell}}{2} \|\mathbf{Z}_{\ell} - \mathbf{W}_{\ell} \mathbf{A}_{\ell-1} + \mathbf{U}_{\ell}\|_F^2 \\ & && + \sum_{\ell=1}^{L-1} \frac{\gamma_{\ell}}{2} \|\mathbf{A}_{\ell} - \phi_{\ell}(\mathbf{Z}_{\ell}) + \mathbf{V}_{\ell}\|_F^2 \end{aligned}$$

where $\beta_{\ell}, \gamma_{\ell} > 0$ are the step sizes, \mathbf{U}_{ℓ} and \mathbf{V}_{ℓ} are the (*scaled dual variables*) [Boyd *et al.*, 2011] for the equality constraint at the layer ℓ . Algorithm 3 shows a standard ADMM scheme for optimizing Eq. (11). Note, the parameters are updated in a closed-form as analytical solution can be simply derived. For simplicity of the equations, we denote $\mathcal{P}_{\ell}(\cdot) = \frac{\beta_{\ell}}{2} \|\mathbf{Z}_{\ell} -$

$\mathbf{W}_{\ell} \mathbf{A}_{\ell-1} + \mathbf{U}_{\ell}\|_F^2$ and $\mathcal{Q}_{\ell}(\cdot) = \frac{\gamma_{\ell}}{2} \|\mathbf{A}_{\ell} - \phi_{\ell}(\mathbf{Z}_{\ell}) + \mathbf{V}_{\ell}\|_F^2$. This algorithm is similar to [Taylor *et al.*, 2016; Wang *et al.*, 2019a] with the difference that all the equality constraints in problem (10) are enforced using multipliers, while previous work only enforced the constraints on the last layer L while other constraints were only loosely enforced using quadratic penalty.

Algorithm 3 Standard ADMM for DNN Training

Input: data \mathbf{X} , labels \mathbf{Y}
Params: $\beta_{\ell} > 0, \gamma_{\ell} > 0, \lambda_{\ell} > 0$
Initialize: $\{\mathbf{W}_{\ell}^0\}_{\ell=1}^L, \{\mathbf{U}_{\ell}^0\}_{\ell=1}^L, \{\mathbf{V}_{\ell}^0\}_{\ell=1}^{L-1}, \{\mathbf{Z}_{\ell}^0\}_{\ell=1}^L, \{\mathbf{A}_{\ell}^0\}_{\ell=1}^{L-1}$ $k \leftarrow 0$
repeat
 for $\ell = 1$ **to** L **do**
 $\mathbf{W}_{\ell}^{k+1} \leftarrow \arg \min \{\mathcal{P}_{\ell}(\cdot) + \lambda_{\ell} \mathbf{r}_{\ell}(\mathbf{W}_{\ell}^k)\}$
 end for
 for $\ell = 1$ **to** $L-1$ **do**
 $\mathbf{Z}_{\ell}^{k+1} \leftarrow \arg \min \{\mathcal{P}_{\ell}(\cdot) + \mathcal{Q}_{\ell}(\cdot)\}$
 $\mathbf{A}_{\ell}^{k+1} \leftarrow \arg \min \{\mathcal{P}_{\ell+1}(\cdot) + \mathcal{Q}_{\ell}(\cdot)\}$
 end for
 $\mathbf{Z}_L^{k+1} \leftarrow \arg \min \{\mathcal{J}(\mathbf{Y}, \mathbf{Z}_L^k) + \mathcal{P}_L(\cdot)\}$
 for $\ell = 1$ **to** $L-1$ **do**
 $\mathbf{U}_{\ell}^{k+1} \leftarrow \mathbf{U}_{\ell}^k + \mathbf{Z}_{\ell}^{k+1} - \mathbf{W}_{\ell}^{k+1} \mathbf{A}_{\ell-1}^{k+1}$
 $\mathbf{V}_{\ell}^{k+1} \leftarrow \mathbf{V}_{\ell}^k + \mathbf{A}_{\ell}^{k+1} - \phi_{\ell}(\mathbf{Z}_{\ell}^{k+1})$
 end for
 $\mathbf{U}_L^{k+1} \leftarrow \mathbf{U}_L^k + \mathbf{Z}_L^{k+1} - \mathbf{W}_L^{k+1} \mathbf{A}_{L-1}^{k+1}$
until some stopping criterion is reached.

While the standard ADMM Algorithm 3 has potentials in training (simple) DNNs [Taylor *et al.*, 2016], there exists hurdles that confines extending ADMM to more complex problems — the global convergence proof of the ADMM [Deng and Yin, 2016] assumes that \mathcal{J} is deterministic and the global solution is calculated at each iteration of the cyclic parameter updates. This makes standard ADMM computationally expensive thus impractical for training of many large-scale optimization problems. Specifically, for deep learning, this would impose a severe restriction on training set size when limited computational resources are available. In addition, since the variable updates in standard ADMM are analytically driven, the extent of its applications is limit to trivial tasks [Taylor *et al.*, 2016], making it incompetent to perform on par with the recent complex architectures introduced in deep learning (*e.g.* [He *et al.*, 2016]).

B Proof for Proposition 1

We follow the steps in the proof for similar problems in [Fu *et al.*, 2018] and [Shi *et al.*, 2017] with deterministic primal updates. Proper modifications are made to cover the stochastic primal update in our proof.

Note that we have

$$\nabla \mathcal{L}_{\rho_k}(\mathbf{X}^k) = \nabla f(\mathbf{X}^k) + \nabla h(\mathbf{X}^k)^T \boldsymbol{\mu}^k,$$

where

$$\boldsymbol{\mu}^k = (1/\rho_k)h(\mathbf{X}^k) + \boldsymbol{\lambda}^k.$$

Our first step is to show that $\{\boldsymbol{\mu}^k\}$ is a convergent sequence. To see this, we define

$$\bar{\boldsymbol{\mu}}^k = \frac{\boldsymbol{\mu}^k}{\|\boldsymbol{\mu}^k\|}.$$

Since $\bar{\boldsymbol{\mu}}^k$ is bounded, it converges to a limit point $\bar{\boldsymbol{\mu}}$. Also let \mathbf{x}^* be a limit point of \mathbf{x}^k . Because we have assumed that

$$\varepsilon_k \rightarrow 0, \quad \sigma_k^2 \rightarrow 0,$$

it means that the mean and variance of the stochastic gradient of our primal update goes to zero. Since our stochastic gradient is unbiased, we have

$$\mathcal{G}(\mathbf{X}^k) \rightarrow \nabla \mathcal{L}_{\rho_k}(\mathbf{X}^*).$$

This also means that we must have $\mathcal{G}(\mathbf{x}^k) \rightarrow \mathbf{0}$ and

$$\nabla L_{\rho_k}(\mathbf{x}^k) \rightarrow \mathbf{0}.$$

Hence, the following holds when $k \rightarrow \infty$:

$$\nabla L_{\rho_k}(\mathbf{X}^*) = \nabla f(\mathbf{X}^*) + \nabla h(\mathbf{X}^*)^T \boldsymbol{\mu}^\infty = \mathbf{0}, \quad (12)$$

Suppose $\boldsymbol{\mu}^k$ is unbounded. By dividing eq. (12) by the above $\|\boldsymbol{\mu}^k\|$ and considering $k \rightarrow \infty$, we must have

$$\nabla h(\mathbf{X}^*)^T \bar{\boldsymbol{\mu}} = \mathbf{0}, \quad \forall \mathbf{X}. \quad (13)$$

The term $\nabla f(\mathbf{X}^*)/\|\boldsymbol{\mu}\|$ is zero since we assumed $\bar{\boldsymbol{\mu}}$ is unbounded. Since $h(\mathbf{X}) = \mathbf{0}$ satisfies the Robinson’s condition, then, for any \mathbf{w} , there exists $\beta > 0$ and \mathbf{x} such that

$$\mathbf{w} = \beta \nabla h(\mathbf{X}^*)(\mathbf{X} - \mathbf{X}^*).$$

This together with eq. (13) says that $\bar{\boldsymbol{\mu}} = \mathbf{0}$. This contradicts to the fact $\|\bar{\boldsymbol{\mu}}\| = 1$. Hence, $\{\boldsymbol{\mu}^k\}$ must be a bounded sequence and thus admits a limit point. Denote $\boldsymbol{\mu}^*$ as this limit point, and take limit of both sides of eq. (12). We have:

$$\nabla f(\mathbf{X}^*) + \nabla h(\mathbf{X}^*)^T \boldsymbol{\mu}^* = \mathbf{0}, \quad \forall \mathbf{X}. \quad (14)$$

In addition, since

$$\rho_k(\boldsymbol{\mu}^k - \boldsymbol{\lambda}^k) = h(\mathbf{X}^k)$$

with $\rho_k \rightarrow 0$ or $\boldsymbol{\mu}^k - \boldsymbol{\lambda}^k \rightarrow 0$ (per our updating rule and $\eta_k \rightarrow 0$), the constraints will be enforced in the limit. \square

C Supervised training of DNNs

Fashion-MNIST. To compare our method with dlADMM [Wang *et al.*, 2019a], we evaluated the performance of our method on the Fashion-MNIST dataset [?] with 60,000 training samples and 10,000 testing samples. We followed the settings in [Wang *et al.*, 2019a] by having 2 hidden layers with 1000 neurons each, and Cross-Entropy loss at the final layer. Also, the batch size is set to 128, $\beta_t = 1$, and the updates for \mathbf{Z}_t and Θ_t (eq. 6a) are performed 3 times at each epoch. Figure 6 shows the test set accuracy results over 200 epochs of training. It can be noticed that Stochastic Block ADMM is converging at lower epochs and reaching a higher test accuracy while performing efficient mini-batch updates. Further, in section C., it will be demonstrated that Stochastic Block

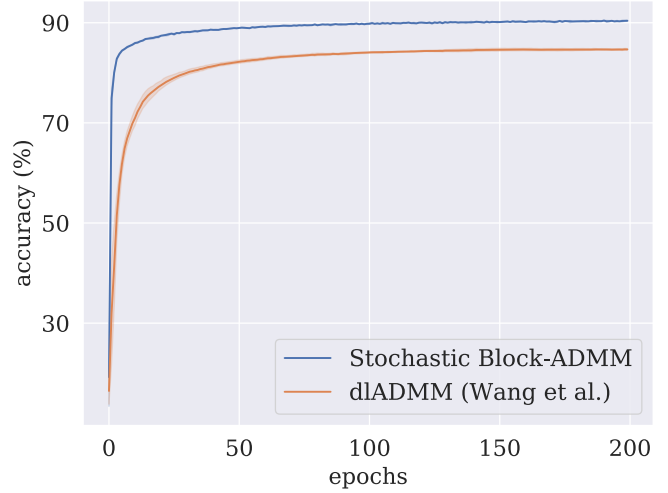


Figure 6: Test accuracy comparison of Stochastic Block ADMM and dlADMM on Fashion-MNIST dataset using a network with 3 fully-connected layers: 784 – 1000 – 1000 – 10. Final test accuracy: “Stochastic Block ADMM”: 90.39%, “Wang *et al.*”:84.67% (averaged over 5 runs).

ADMM converges drastically faster than dlADMM in terms of wall clock time.

CIFAR-10. The previous works on training deep networks using ADMM have been limited to trivial networks and datasets (e.g. MNIST) [Taylor *et al.*, 2016; Wang *et al.*, 2019a]. However, our proposed method does not have many of the existing restrictions and assumptions in the network architecture, as in previous works do, and can easily be extended to train non-trivial applications. It is critical to validate stochastic block-ADMM in settings where deep and modern architectures such as deep residual networks, convolutional layers, cross-entropy loss function, etc., are used. To that end, we validate the ability of our method in a supervised setting (image classification) on the CIFAR-10 dataset [Krizhevsky *et al.*,] using ResNet-18 [He *et al.*, 2016]. To best of our knowledge, this is the first attempt of using ADMM for training complex networks such as ResNets.

For this purpose, we used 50,000 samples for training and the remaining 10,000 for evaluation. To have a fair comparison, we followed the configuration suggested in [Gotmare *et al.*, 2018] by converting Resnet-18 network into two blocks ($T = 2$), with the splitting point located at the end of CONV3_X layer. We used the Adam optimizer to update both the blocks and the decoupling variables with the learning rates of $\eta_t = 5e^{-3}$ and $\zeta_t = 0.5$. We noted since the auxiliary variables \mathbf{Z}_t are not “shared parameters” across data samples, they usually require a higher learning rate in Algorithm 1. Also, we found the ADMM step size $\beta_t = 1$ to be sufficient for enforcing the block’s coupling.

Figure. 7 shows the results from our method compared with two baselines: [Gotmare *et al.*, 2018], and conventional end-to-end neural network training using back-propagation and SGD. Our algorithm consistently outperformed [Gotmare *et al.*, 2018] however cannot match the conventional

SGD results. There are several factors that we hypothesize that might have contributed to the performance difference: 1) in a ResNet the residual structure already partially solved the vanishing gradient problem, hence SGD/Adam performs significantly better than a fully-connected version; 2) we noticed decreasing the learning rate for Θ_t updates does not impact the performance as it does for an end-to-end back-propagation using SGD. Still, we obtained the best performance of ADMM-type methods on both MNIST and CIFAR datasets, showing the promise of our approach.

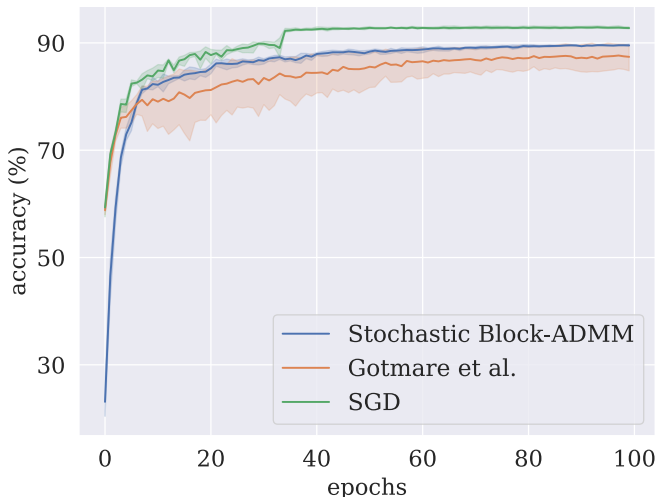


Figure 7: Test set accuracy on CIFAR-10 dataset. Final accuracy "Block ADMM": 89.66%, "Gotmare *et al.*":87.12%, "SGD": **92.70%**. (Best viewed in color.)

D Weakly Supervised Attribute Prediction

Factorizing the activations

With the assumption that the observations are formed by a linear combination of few basis vectors, one can approximate a given matrix $\mathbf{X} \in \mathbb{R}^{m \times n}$ into a *basis* matrix $\mathbf{M} \in \mathbb{R}^{m \times r}$ and an *score* matrix $\mathbf{S} \in \mathbb{R}^{r \times n}$ such that $\mathbf{X} \approx \mathbf{M}\mathbf{S}$ where r is the (reduced) *rank* of the factorized matrices – commonly $r \ll \min(m, n)$. Methods such as NMF would restrict the entries of \mathbf{M} and \mathbf{S} to be non-negative ($\forall i, j \mathbf{M}_{ij} \geq 0, \mathbf{S}_{ij} \geq 0$) which forces the decomposition to be only *additive*. This has been shown to result in a parts-based representation that is intuitively more close to human perception. It is also worth mentioning that obviously, the matrix \mathbf{X} needs to be positive ($\forall i, j \mathbf{X}_{ij} \geq 0$). For non-negative factorization on the activations of the DNNS, due to the common use of activation functions such as *ReLU*, this would not impose any constraints in most of the problems.

Activations of the CNN networks are generally tensors of the shape $\mathbf{Z}_\ell \in \mathbb{R}^{(N,C,H,W)}$ which namely represent the batch size of the input, the number of the channels, the height of each channel, and the corresponding width. To adapt such tensors for the NMF problem, we reshape the tensor into the matrix $\mathbf{Z}_\ell \in \mathbb{R}^{C \times (N*H*W)}$ by stacking it over its channels

while flattening the other dimensions. This way, the channels would be embedded into a pre-defined small dimension r while keeping each sample and pixels information. For the weakly-supervised problem of attribute classification using DeepFacto, we attached the DeepFacto module to the last convolutional layer of the Inception-Resnet-V1 architecture followed by a *ReLU*. This layer has 1792 channels and, for a given input of the size 160×160 pixels (the original input size from the LFWA dataset), the height and the width are both equal to 3.

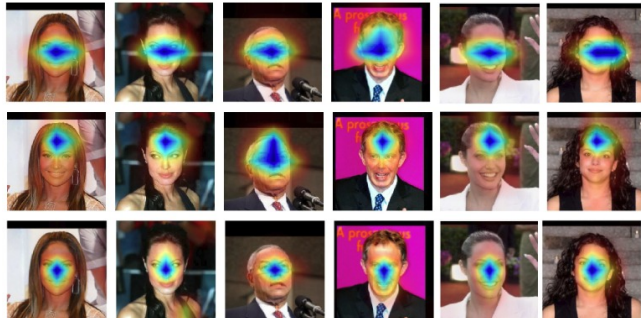


Figure 8: Heat map visualizations from three different dimensions of the score matrix \mathbf{S} (rows) trained by DeepFacto-32 over different samples (columns) in LFWA dataset. These dimensions can capture interpretable representations over different faces identities: *eyes* (top), *forehead* (middle), and *nose* (bottom).

Heat maps

To qualitatively investigate the interpretability of the factorized representations learned from DeepFacto, similar to [Collins *et al.*, 2018], one can visualize the score matrix \mathbf{S} . Each dimension of the score matrix \mathbf{S} can be reshaped back to the original activation size and be up-sampled to the size of the input using bi-linear interpolation. In Figure 8, the score matrix learned from the DeepFacto with $r = 32$ (average attribute prediction of 81.4%) is used where three different heat maps (out of 32) are depicted over different samples from LFWA dataset. We have found $r = 4$ to be very low to represent interpretable heat maps for the attributes and $r = 256$ to contain redundant heat maps. It can be seen, that the heat maps can show local and persistent attention over different face identities: *eyes, forehead, nose*, etc.

Table 2: Prediction accuracy (%) of individual attributes in LFWA dataset. DeepFacto with other weakly-supervised and supervised baselines.

ATTRIBUTES	DEEFACTO			[LIU <i>et al.</i> , 2015]	[LIU <i>et al.</i> , 2018]	[ZHANG <i>et al.</i> , 2014]
	(WEAKLY-SUPERVISED)			(WEAKLY-SUPERVISED)	(SUPERVISED)	(SUPERVISED)
	$r = 256$	32	4			
'5 O CLOCK SHADOW'	83.3	80.0	68.7	78.8	84	84
'ARCHED EYEBROWS'	86.6	83.9	79.2	78.1	82	79
'ATTRACTIVE'	84.3	79.8	73.3	79.2	83	81
'BAGS UNDER EYES'	83.9	72.5	64.5	83.1	83	80
'BALD'	94.3	93.3	89.3	84.8	88	84
'BANGS'	93.2	88.4	84.4	86.5	88	84
'BIG LIPS'	83.2	77.0	71.9	75.2	75	73
'BIG NOSE'	80.1	68.7	61.4	81.3	81	79
'BLACK HAIR'	92.7	91.4	87.4	87.4	90	87
'BLOND HAIR'	97.9	97.3	93.2	94.2	97	94
'BLURRY'	90.4	90.5	86.5	78.4	74	74
'BROWN HAIR'	78.4	74.4	70.2	72.9	77	74
'BUSHY EYEBROWS'	84.0	78.6	63.4	83.0	82	79
'CHUBBY'	80.5	75.2	71.1	74.6	73	69
'DOUBLE CHIN'	86.0	77.9	72.3	80.2	78	75
'EYEGASSES'	94.3	89.6	84.8	89.5	95	89
'GOATEE'	89.1	85.4	80.0	78.6	78	75
'GRAY HAIR'	91.9	90	85.6	86.9	84	81
'HEAVY MAKEUP'	96.3	91.5	87.4	94.5	95	93
'HIGH CHEEKBONES'	90.4	79.0	72.1	88.8	88	86
'MALE'	81.3	76.6	70.5	94.3	94	92
'MOUTH SLIGHTLY OPEN'	85.4	78.0	73.3	81.7	82	78
'MUSTACHE'	96.6	93.2	91.3	83.3	92	87
'NARROW EYES'	78.3	69.3	58.4	77.5	81	73
'NO BEARD'	79.5	73.0	65.5	77.7	79	75
'OVAL FACE'	80.6	73.2	66.1	78.7	74	72
'PALE SKIN'	75.1	66.7	60.6	89.8	84	84
'POINTY NOSE'	81.6	73.7	62.2	79.8	80	76
'RECEDING HAIRLINE'	84.0	80.9	73.8	88.0	85	84
'ROSY CHEEKS'	87.3	87.4	83.4	79.9	78	73
'SIDEURNS'	85.4	81.5	75.8	80.5	77	76
'SMILING'	92.6	78.7	69.8	92.2	91	89
'STRAIGHT HAIR'	82.8	77.0	72.1	73.6	76	73
'WAVY HAIR'	80.4	77.0	68.3	81.7	76	75
'WEARING EARRINGS'	95.4	91.6	87.1	89.7	94	92
'WEARING HAT'	93.0	90.2	87.0	80.5	88	82
'WEARING LIPSTICK'	95.8	92.8	89.0	91.4	95	93
'WEARING NECKLACE'	93.0	89.8	85.1	84.0	88	86
'WEARING NECKTIE'	79.8	75.2	70.6	78.7	79	79
'YOUNG'	91.0	88.4	84.4	79.2	86	82
AVERAGE	87.0	81.4	74.8	83.1	84	81